2017

X-Tream dosimetry of highly brilliant X-ray microbeams in the MRT hutch of the Australian Synchrotron

Pauline Fournier
University of Wollongong, pf891@uowmail.edu.au

Iwan Cornelius
University of Wollongong, iwan@uow.edu.au

Andrew Dipuglia
University of Wollongong, ad150@uowmail.edu.au

Matthew Cameron
University of Wollongong, mc815@uowmail.edu.au

Jeremy A. Davis
University of Wollongong, jeremyd@uow.edu.au

See next page for additional authors

X-Tream dosimetry of highly brilliant X-ray microbeams in the MRT hutch of the Australian Synchrotron

Abstract

The X-Tream dosimetry system developed at the Centre for Medical Radiation Physics (University of Wollongong, Australia) utilises a high resolution silicon Single Strip Detector to characterise synchrotron radiation microbeams for the purpose of Quality Assurance of Microbeam Radiation Therapy. Firstly, a comparison of the Silicon Strip Detector performance with respect to a conventional PinPoint Ionisation Chamber for broad beams and microbeams is given. These results are then extended to characterise the horizontal microbeam radiation field available in the high flux experimental hutch of the Imaging and Medical BeamLine at the Australian Synchrotron. The Silicon Strip Detector measured depth dose curve of the broad beam agrees very well with the PinPoint Ionisation Chamber measurements between 10 and 50 mm depth in water. Significant deviations from the PinPoint Ionisation Chamber response are observed with increasing depth. Microbeam profiles measured by the Silicon Strip Detector are well resolved but clearly affected by misalignment of the Silicon Strip Detector with respect to the microbeams. Future beamline technical improvements will alleviate this issue.

Disciplines

Engineering | Science and Technology Studies

Publication Details

Fournier, P., Cornelius, I., Dipuglia, A., Cameron, M., Davis, J. A., Cullen, A., Petasecca, M., Rosenfeld, A. B., Brauer-Krisch, E., Hausermann, D., Stevenson, A. W., Perevertaylo, V. & Lerch, M. L. F. (2017). X-Tream dosimetry of highly brilliant X-ray microbeams in the MRT hutch of the Australian Synchrotron. Radiation Measurements, 106 405-411.

Authors

Pauline Fournier, Iwan Cornelius, Andrew Dipuglia, Matthew Cameron, Jeremy A. Davis, Ashley Cullen, Marco Petasecca, Anatoly B. Rosenfeld, Elke Brauer-Krisch, Daniel Hausermann, Andrew W. Stevenson, Vladimir Perevertaylo, and Michael L. F Lerch

X-tream dosimetry of highly brilliant X-ray microbeams in the MRT hutch of the Australian Synchrotron

Pauline Fournier[a], Iwan Cornelius[a,d], Andrew Dipuglia[a], Matthew Cameron[a], Jeremy A. Davis[a], Ashley Cullen[a], Marco Petasecca[a,b], Anatoly B. Rosenfeld[a,b], Elke Bräuer-Krisch[c], Daniel Häusermann[d], Andrew W. Stevenson[d], Vladimir Perevertaylo[e], Michael L. F. Lerch[a,b]

[a]*Centre for Medical Radiation Physics, University of Wollongong, Northfields Avenue, Gwynneville N.S.W 2500, Australia*
[b]*Illawarra Health Medical Research Institute, University of Wollongong, Northfields Avenue, Gwynneville N.S.W 2500, Australia*
[c]*European Synchrotron Radiation Facility (ESRF), 71 Avenue des Martyrs, 38000 Grenoble, France*
[d]*Australian Synchrotron, 800 Blackburn Rd, Clayton VIC 3168, Australia*
[e]*SPA BIT, Kiev 01004, Ukraine*

Abstract

The X-Tream dosimetry system developed at the Centre for Medical Radiation Physics (University of Wollongong, Australia) utilises a high resolution silicon Single Strip Detector to characterise synchrotron radiation microbeams for the purpose of Quality Assurance of Microbeam Radiation Therapy. Firstly, a comparison of the Silicon Strip Detector performance with respect to a conventional PinPoint Ionisation Chamber for broad beams and microbeams is given. These results are then extended to characterise the horizontal microbeam radiation field available in the high flux experimental hutch of the Imaging and Medical Beam-Line at the Australian Synchrotron. The Silicon Strip Detector measured depth dose curve of the broad beam agrees very well with the PinPoint Ionisation Chamber measurements between 10 and 50 mm depth in water. Significant deviations from the PinPoint Ionisation Chamber response are observed with increasing depth. Microbeam profiles measured by the Silicon Strip Detector are well resolved but clearly affected by misalignment of the Silicon Strip Detector with respect to the microbeams. Future beamline technical improvements will alleviate this issue.

Keywords: Microbeam radiation therapy (MRT) , Dosimetry, Quality Assurance (QA).

1. Introduction

Synchrotron Microbeam Radiation Therapy (MRT) is a novel radiotherapy technique targeted at treating inoperable tumours in children. The MRT modality makes use of highly brilliant synchrotron X-rays passing through a Multi-Slit Collimator (MSC) to create a spatially fractionated array of X-ray Micro Beams (MB) with width of approximately 25 to 100 $\mu\mathrm{m}$ and pitch of 100 to 400 $\mu\mathrm{m}$, where the MB width and pitch depend upon the dimensions of the MSC and distance from MSC to target. The major physical benefit of this approach lies in the dose volume effect: a higher radiation tolerance of the normal tissue when using micrometre scale beam size [1] [2] [3]. Such tolerance is not observed for cancer tissue [4], which leads to a natural differential effect in the MRT approach. Using MRT thus implies an extraordinary sparing of the normal tissue. One of the possible applications of MRT, is the treatment of inoperable and very radiation resistant paediatric brain tumours where conventional radiotherapy presents a high level of toxicity on the developing brain [5] [6] [7].

The MRT technique is currently under development at the Imaging and Medical Beam Line (IMBL) at the

Australian Synchrotron, and showing very promising results [8]. As with all radiotherapy treatments, MRT requires dedicated quality assurance (QA) procedures which necessitates the use of specialised dosimetric systems. The experimental dosimetry of the microbeams is a challenging task that requires a detector with large dynamic range (to measure both peak and valley dose accurately), micrometer-scale spatial resolution, real time readout, good radiation hardness (to withstand dose rates up to 20 $\mathrm{kGy\,s^{-1}}$) and ideally waterproof. The shift from the pre-clinical to the clinical trial stage, requires new and novel developments in dosimetry based technologies and methodologies, which is the framework of this study.

A variety of technologies are currently in use at MRT facilities, with Gafchromic film and the PTW microdiamond representing two of the more promising technologies available. Gafchromic film is very well known, having a long history within radiation dosimetry. There are a number of different types of Gafchromic film, with each having a different dynamic range. Regardless of the type, Gafchromic film suffers from one crucial disadvantage with respect to long term applicability to MRT. Given the developing time after radiation exposure, it cannot be used for real time dose monitoring, which is essential for QA. A device which overcomes this disadvantage by offering real time monitoring is the PTW microdiamond dosimeter [9]. The PTW microdiamond is becoming an established device within the small field dosimetry due to its tissue equivalence and radiation hardness, with applicability to MRT fields demonstrated [10]. A critical disadvantage of the device is a lack of sensitivity, when compared with silicon based devices. Due to the geometry of the active layer, the quoted micron scale resolution is subject to degradation unless a rigorous and time-consuming alignment methodology is applied. Lastly, the price of the technology means that deployment will be expensive and therefore, limited.

In this paper, a Silicon Strip Detector (SSD), designed at the Centre for Medical Radiation Physics (CMRP) and fabricated at SPA BIT, Kiev, Ukraine is used to perform a dosimetric analysis of synchrotron radiation at the IMBL. In this work, the SSD is tested in two different configurations; broad beam (BB) and micro beam (MB). The SSD is demonstrated to be able to perform dosimetric measurements of BB and MB in real time, in both water and Gammex-RMI457 solid water phantoms with micron-scale spatial resolution. The MB measurements highlighted the high spatial resolution of the SSD, however, due to misalignment of the detector with respect to MB in the experimental set-up, an over response in the measurement of the Full Width Half Maximum (FWHM) and the Peak to Valley Dose Ratio (PVDR) was observed. SSD measurements are compared to the PinPoint 31014 Ionisation Chamber (IC) [9] in a broad beam radiation field at different depths in water to investigate the impact of expected beam hardening. The results derived from this experiment are promising, but indicative that an improved methodology be developed to mitigate alignment issues and energy dependence of silicon dosimeters.

2. Device Specifics

The SSD consists in a micro-strip diode fabricated via ion implantation on a p-type epitaxial substrate. The single strip dimensions are 900 x 10 $\mu\mathrm{m}^2$. The 100 $\Omega\,\mathrm{cm}$ p-type epitaxial layer is grown on top of a 370 $\mu\mathrm{m}$ thick substrate of lower resistivity (0.001 $\Omega\,\mathrm{cm}$) [8] [11]. A silicon oxide (SiO2) layer surrounds the silicon detector in order to protect the bulk silicon (from dust, oil, grit, etc.) and avoid the generation of surface leakage currents that would otherwise degrade the overall performance of the device. The SSD structure also incorporates a n-type guard ring limiting the width of the sensitive area to approximately 30 $\mu\mathrm{m}$ for an applied bias of -50V [11]. Very high resolution dosimetry can be achieved using the SSD in "edge-on" mode (see Figure 1a) and in active mode using an operating voltage between -50 and -70 V. When using the "edge-on" orientation, the depletion region in the epitaxial growth direction defines the intrinsic width of the sensitive volume. Because of the low resistivity of the silicon, this length can be as low as 10-12 $\mu\mathrm{m}$ at a -30 V polarising voltage [11]. In addition to this, the effect of the guard ring design allows further reduction

in the depletion width as it acts as a sucking electrode to collect a proportion of the charge created directly under the strip electrode.

3. Materials and Methodology

Broad Beam (BB) and Micro Beam (MB) experiments were performed upon the Imaging and Medical Beam Line (IMBL) at the Australian Synchrotron (AS) in Hutch 1B (see Figure 2), which is positioned close to the wiggler source to maximise the dose rate [12]. 'Clean-up' slits are positioned upstream of the sample stage, which is located at around 20 m from the beam source. The vertical slits can define two different beam heights: 1 mm and 2 mm. The maximum lateral field size is limited (by application of an acceptable beam intensity roll-off) to 30 mm at the sample stage.

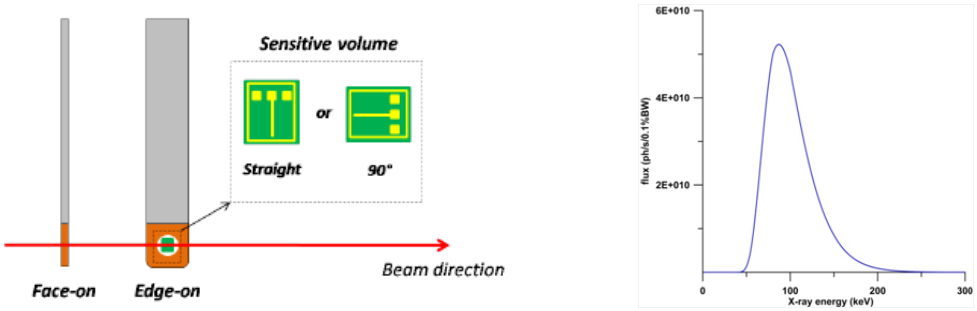

(a) Different possible orientations of the SSD.

(b) Photon energy spectrum.

Figure 1: Different modes of operation for SSD, i.e. Edge-On and Face-On (1a) and photon energy spectra in Hutch 1B (1b) calculated by SPEC [13].

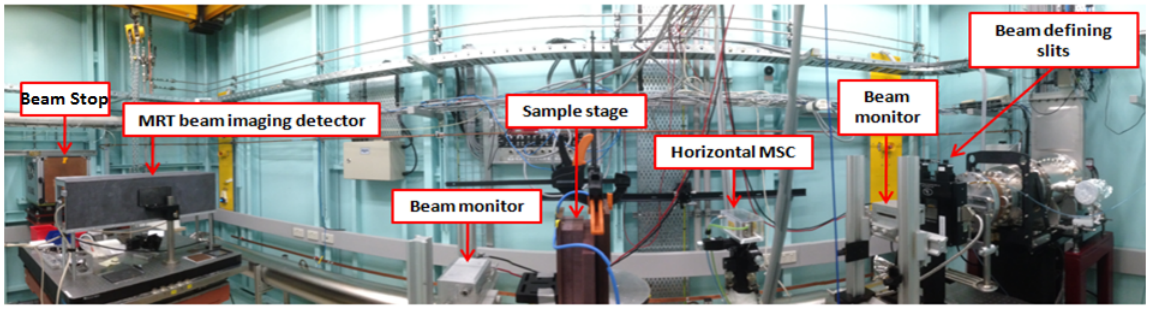

Figure 2: Instrumentation in Hutch 1B at IMBL where the measurements of the horizontal microbeams were performed.

The energy spectrum used during the experiment has been calculated using the SPEC program, developed at the AS for modelling radiation fields produced at the IMBL [13]. The energy spectra was calculated using the parameters presented in Table 1. In order to distribute the heat load over a larger area, the in-vacuo filters were tilted by 45 ° in regard to the incident synchrotron beam [14]. The resulting effective thickness of each filter is given in Table 1 and the resulting energy spectrum is displayed in Figure 1b.
For both the BB and MB configuration, a Pinpoint IC with a sensitive volume of radius 1 mm and length of 5 mm, is used to provide a reference in terms of dosimetry.

Parameter	Value
Electron energy in the storage ring	3.032 GeV
Storage ring current	200 mA
Peak magnetic field	3 T
Clean up slits aperture	1 mm x 1 mm
Distance from the source	22 m
Filtration in hutch 1A	+ 10 mm C at 45° (Eq. thickness = 14.14 mm)
	+ 1 mm Al at 45° (Eq. thickness = 1.41 mm)
	+ 2 mm Cu at 45° (Eq. thickness = 2.83 mm)
Filtration in hutch 1B	+ 0.35 mm Be
	1 m air

Table 1: Parameters used for the calculation in SPEC.

3.1. Broad Beam (BB) Configuration

Measurements were performed for both Pinpoint IC and SSD at multiple depths in both water and Gammex-RMI457 solid water phantoms (see Fig. 3 and 4) in a 20 mm x 2 mm beam. The beam is scanned vertically to create an effective field size of 20 x 20 mm^2 which is the recommended by the manufacturer [9]. Care was taken to ensure that the middle of the active area of the IC was centred at the middle of the irradiation field at each depth. Depth dose profiles were calculated and normalised to the measured response at an appropriate reference depth.

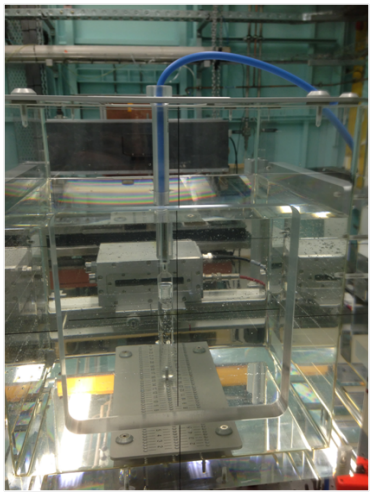

Figure 3: PinPoint in Water tank.

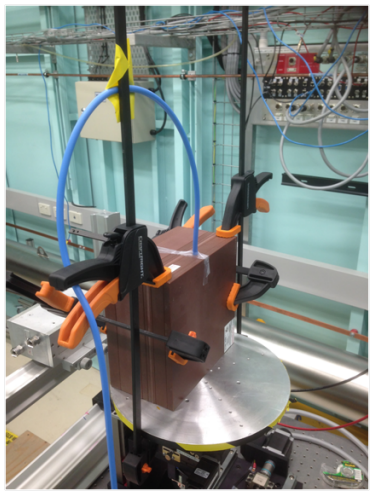

Figure 4: PinPoint in Solid water phantom.

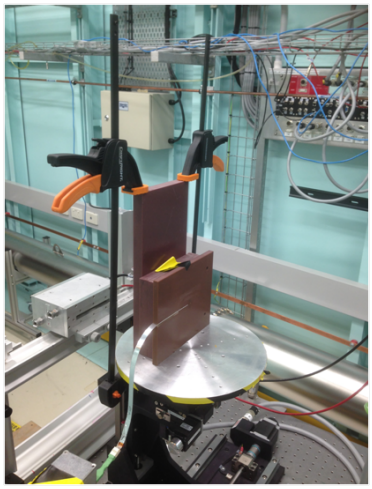

Figure 5: SSD set-up in edge-on mode

3.2. Micro Beam (MB) Configuration

The MSC available in hutch 1B creates horizontal Micro Beams (MB). The MSC is made of several tungsten carbide plates separated by kapton foils of different thickness's which define the MB apertures and thus the MB width. This MSC permits two MB setting configurations named hereafter as 25-200 and 50-200.

The 25-200 MSC configuration generates 25 μm FWHM microbeams separated by a 200 μm Peak-To-Peak distance. Conversely, the 50-200 configuration generates 50 μm FWHM microbeams separated by a 200 μm Peak-To-Peak distance. The experiments consisted of the acquisition of microbeams profiles for both MSC configurations using the SSD. The SSD was fixed in a dedicated Gammex plate (see Figure 5) and vertical profiles were acquired at different depths within the Gammex-RMI457 solid water phantom. A 10 mm x 1 mm field size was used and the vertical profiles were acquired with 5 $\mathrm{mm\,s^{-1}}$ vertical scan speed. A bias of -70V was applied across the SSD.

4. Results

4.1. Broad Beam (BB) Configuration

The signal from the SSD and PinPoint IC was measured at different depths in water for 20 mm x 2 mm beam and are compared in Figure 6. For both detectors, the signal is normalised to 100% at the reference depth of 20 mm. For an additional interpretation we have also normalised the broad beam responses at a depth of 250 mm in water in Figure 7 [15]. The relative difference of the SSD signal relative to the PinPoint is defined as:

$$\Delta = 100\frac{SSD(x) - PinPoint(x)}{PinPoint(x)} \tag{1}$$

where SSD(x) and PinPoint(x) respectively are the SSD and the PinPoint normalised signal at the depth x. Δ is represented by the black dots in Figure 6. At shallow depths, the SSD signal is lower than the PinPoint but the relative difference remains below -2%. From 70 mm depth, the magnitude of the relative difference is increasing with depth up to -36.3% at 250 mm depth. The SSD has a strong energy dependence for photon beam energies below 150 keV. As a result, the SSD is expected to be more water equivalent at greater depths where the contribution of low energy photons is less (i.e. where the energy spectrum is harder). Since the MRT reference depth is 20 mm, SSD measurements at depths where significant beam hardening occurs (i.e. deeper than 50 mm) therefore appear to under-respond compared to the PinPoint IC (see Figure 6). In Figure 7 the SSD and PinPoint signals are normalised to 100% at the greatest depth (i.e 250 mm) in order to better emphasise the impact of the SSD energy dependence.

From 250 mm depth to 70 mm, the SSD over-response goes from 0 to 47.8%. For shallower depths, the difference remains around 55%. The constant over-response, while not ideal, implies that only a single calibration factor is required for depths between 10 and 50 mm for QA of the MRT treatment verification in the water tank.

4.2. Micro Beam (MB) Configuration

The vertical profile obtained with the SSD at 20 mm depth in the Gammex-RMI457 solid water phantom, for the 25-200 MSC configuration is displayed in Figure 8. The beam height was limited to 1 mm, so as limit the scan to only four microbeams. A FWHM of 59 μm was found instead of the expected value of 25 μm, due to the unavoidable misalignment of the detector with the current experimental set-up. Previous MRT experimental measurements done in air using the same SSD have demonstrated a effective spatial resolution of 9 μm [16]. Detector misalignment results in an increased effective sensitive volume size with respect to the incident microbeams, decreasing the SSDs spatial resolution which in turn, leads to a larger FWHM. The FWHM is affected by depth partly due to beam divergence, which results in broadening of microbeams with increased depth. This misalignment of the detector was due to the positioning motors of the sample stage not allowing for high precision in alignment of the detector, relative to the microbeams and no imaging modality

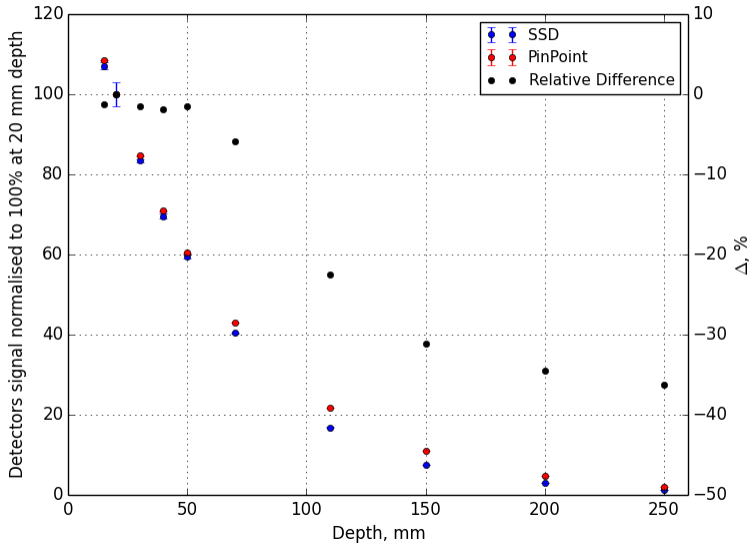

Figure 6: Variation of both PinPoint and SSD signals with depth for a normalisation to 100% at 20 mm depth. The second ordinate axis represents the relative difference of the SSD data to the PinPoint (black dots).

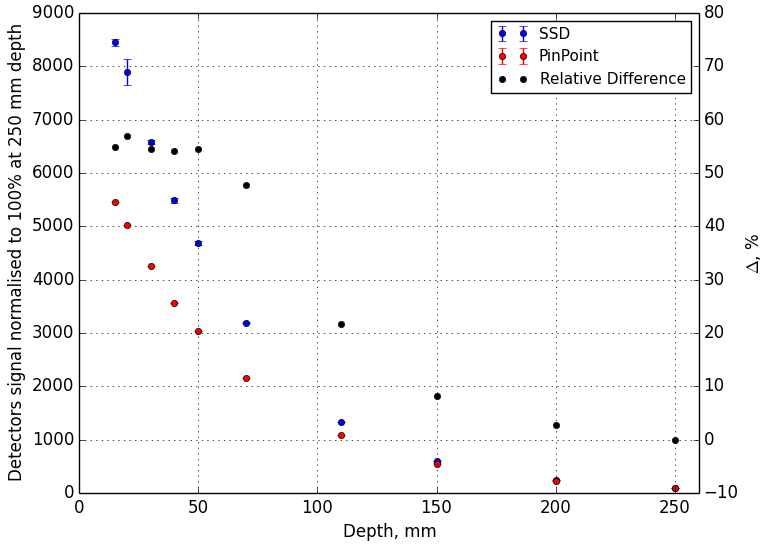

Figure 7: Variation of both PinPoint and SSD signals with depth for a normalisation to 100% at 250 mm depth. The second ordinate axis represents the relative difference of the SSD data to the PinPoint (black dots).

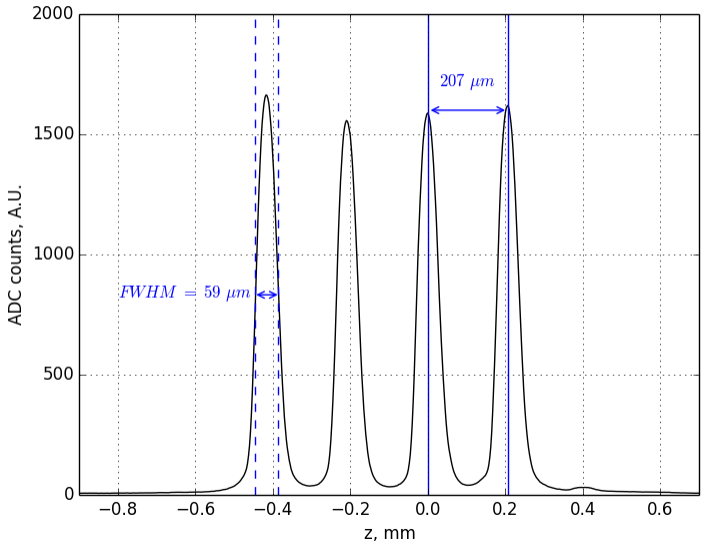

Figure 8: Horizontal microbeams measured with the SSD for 25-200 MSC configuration.

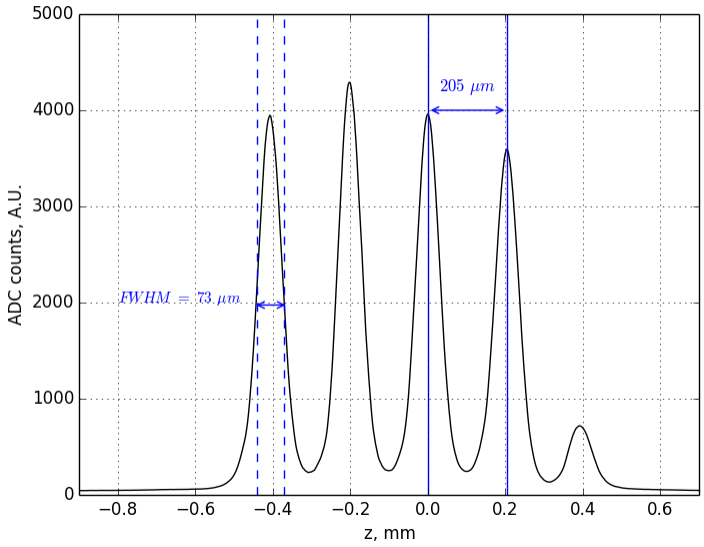

Figure 9: Horizontal microbeams measured with the SSD for 50-200 MSC configuration.

was available to image and align the SSD. Future work will need to have this functionality to increase the accuracy of microbeam measurements.

Similar graphs to those presented in Figure 8 have been obtained for the 50-200 MSC configuration and are presented in Figure 9. Because of the larger microbeam aperture, the impact of the detector misalignment is less, so that the peak and valley signals are higher for the 50-200 MSC configuration when compared to the 25-200 MSC configuration. At each depth investigated, the four peaks values have been averaged as well as the three valley values and the resulting peak-to-valley dose ratio (PVDR) data is presented as a function of depth in Figure 10 and Figure 11. The PVDR is observed to remain approximately constant with depth. This will be verified via Monte Carlo radiation transport simulations in the future.

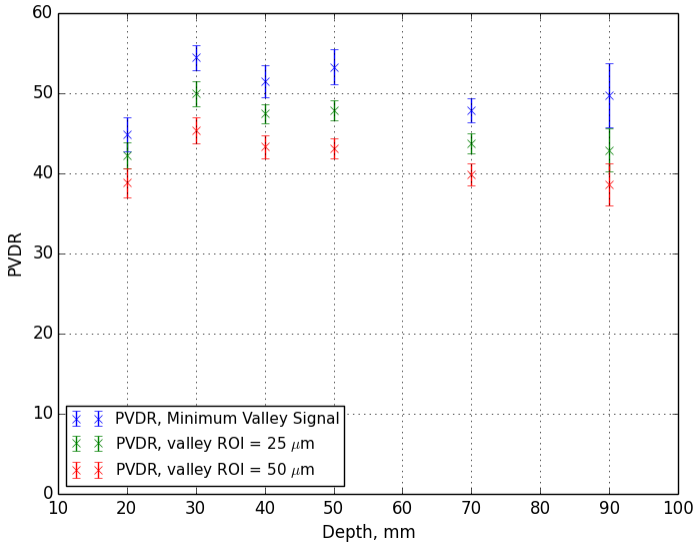

Figure 10: PVDRs obtained for the 25-200 MSC configurations, for a valley either equal to the minimum value between two consecutive peak (blue crosses) or equal to the average signal over an ROI of 25 µm (green crosses) or 50 µm (red crosses) centred between two consecutive peaks.

5. Discussion

5.1. Broad Beam (BB) Configuration

Broadbeam experiments were performed in the MRT hutch (hutch 1B) on the IMBL at the Australian Synchrotron. In this study the results obtained with the reference dosimeter at IMBL (i.e. the PinPoint IC) have been compared to the SSD. Broadbeam measurements were performed at different depths in a water phantom. The SSD energy dependence was highlighted in the measurements performed at different depths in water when compared to the PinPoint IC results. Depth dose curves were obtained with the PinPoint IC in a water phantom. Verification of percentage depth dose profiles and the IMBL energy spectrum using MC simulations will be the subject of future work. The impact of the non-standard irradiation field size on the measured depth dose profile using the IC will also be investigated.

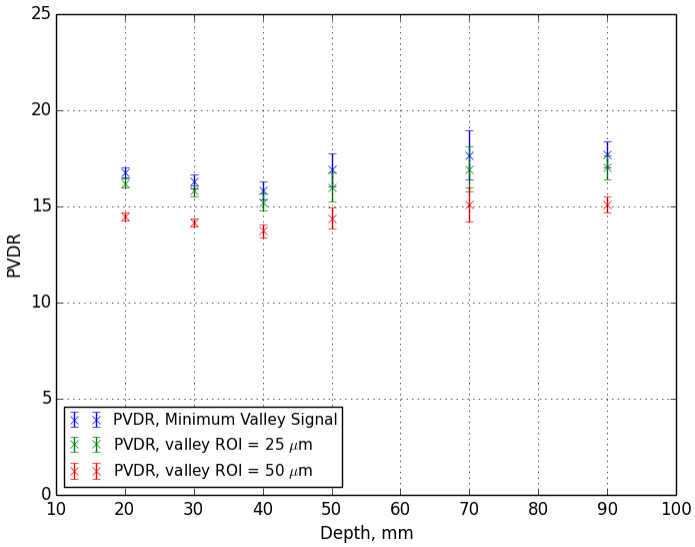

Figure 11: PVDRs obtained for the 50-200 MSC configurations, for a valley either equal to the minimum value between two consecutive peak (blue crosses) or equal to the average signal over an ROI of 25 µm (green crosses) or 50 µm (red crosses) centred between two consecutive peaks.

5.2. Micro Beam (MB) Configuration

Horizontal microbeams intensity profiles have been measured at different depths within a Gammex-RMI457 solid water phantom for both the 25-200 and 50-200 MSC configurations. Due to the lack of SSD alignment possibilities at the IMBL beam line of the Australian Synchrotron, at the time of these measurements (beam line is still under construction) the measured FWHM of the microbeams were higher than expected (59 µm and 73 µm measured FWHM instead of the 25 µm and 50 µm expected values). However, the Peak-To-Peak distances measured (207 µm and 205 µm for 25- 200 and 50-200 MSC configuration respectively) were in agreement with the 200 µm expected value. Different ROIs were considered for the valley definition and the effect on the resulting PVDRs was investigated. The results showed that the valley was not uniform even in small regions between two consecutive peaks. Consequently, it would be important for future studies to define the valley region depending on the microbeams width and pitch, as this can have a significant effect on the PVDR and therefore on the expected normal tissue tolerance.

6. Conclusion

In this study, measurements of highly intense X-rays in both broadbeam (BB) and microbeam (MB) configurations were performed using first generation silicon strip detectors (SSD) at the Australian Synchrotron. The SSD was used to measure the full width half maximum (FWHM) and peak to valley dose ratio (PVDR) of MBs having peak widths of 25 and 50 µm with pitch of 200 µm. Due to some misalignment and energy dependence, an over response in FWHM measurements was observed. Upgrades at the IMBL (vertical and horizontal laser alignment system), along with an improved experimental methodology, have minimised alignment issues for future work. Despite the aforementioned over response; the results are

promising, indicative of their applicability in the Quality Assurance (QA) of microbeam radiation therapy (MRT) and serve well as proof of concept. New devices have been produced with reduced active layer thickness and etched surroundings to address these limitations. Given the SSDs radiation hardness and expected micron resolution of next generation SSDs, X-Tream dosimeters based upon SSD technology will be soon be suitable for use in a clinical setting.

References

[1] H. J. Curtis, The Use of a Deuteron Microbeam for Simulating the Biological Effects of Heavy Cosmic-Ray Particles, Radiat. Res. Suppl. 7 (1967) 250. doi:10.2307/3583718.
URL http://www.jstor.org/stable/3583718?origin=crossref

[2] W. Zeman, H. Curtis, E. Gebhard, W. Haymaker, Tolerance of Mouse-Brain Tissue to High-Energy Deuterons, Science (80-.). 130 (3391) (1959) 1760–1761. doi:10.1126/science.130.3391.1760.
URL http://www.sciencemag.org/cgi/doi/10.1126/science.130.3391.1760

[3] W. Zeman, H. J. Curtis, C. P. Baker, Histopathologic Effect of High-Energy-Particle Microbeams on the Visual Cortex of the Mouse Brain, Radiat. Res. 15 (4) (1961) 496. doi:10.2307/3571293.
URL http://www.jstor.org/stable/3571293?origin=crossref

[4] A. Bouchet, B. Lemasson, G. Le Duc, C. Maisin, E. Bräuer-Krisch, E. A. Siegbahn, L. Renaud, E. Khalil, C. Rémy, C. Poillot, A. Bravin, J. A. Laissue, E. L. Barbier, R. Serduc, Preferential Effect of Synchrotron Microbeam Radiation Therapy on Intracerebral 9L Gliosarcoma Vascular Networks, Int. J. Radiat. Oncol. 78 (5) (2010) 1503–1512. doi:10.1016/j.ijrobp.2010.06.021.
URL http://linkinghub.elsevier.com/retrieve/pii/S0360301610008709

[5] M. A. Grotzer, J. Laissue, H. Blattmann, H. P. Wagner, M. A. Grotzer, D. N. Slatkin, Prospects for microbeam radiation therapy of brain tumours in children to reduce neurological sequelae, Dev. Med. Child Neurol. 49 (8) (2007) 577–581. doi:10.1111/j.1469-8749.2007.00577.x.
URL http://doi.wiley.com/10.1111/j.1469-8749.2007.00577.x

[6] K. Ribi, C. Relly, M. A. Landolt, F. D. Alber, E. Boltshauser, M. A. Grotzer, Outcome of Medulloblastoma in Children: Long-Term Complications and Quality of Life, Neuropediatrics 36 (6) (2005) 357–365. doi:10.1055/s-2005-872880.
URL http://www.thieme-connect.de/DOI/DOI?10.1055/s-2005-872880

[7] D. N. Slatkin, P. Spanne, F. A. Dilmanian, M. Sandborg, Microbeam radiation therapy., Med. Phys. 19 (6) (1992) 1395. doi:10.1118/1.596771.
URL http://scitation.aip.org/content/aapm/journal/medphys/19/6/10.1118/1.596771

[8] M. Lerch, M. Petasecca, A. Cullen, A. Hamad, H. Requardt, E. Bräuer-Krisch, A. Bravin, V. Perevertaylo, A. Rosenfeld, Dosimetry of intensive synchrotron microbeams, Radiat. Meas. 46 (12) (2011) 1560–1565. doi:10.1016/j.radmeas.2011.08.009.
URL http://dx.doi.org/10.1016/j.radmeas.2011.08.009http://linkinghub.elsevier.com/retrieve/pii/S1350448711004215

[9] PTW.
URL http://www.ptw.de/2253.html

[10] J. Livingstone, A. W. Stevenson, D. J. Butler, D. Häusermann, J.-f. Adam, Characterization of a synthetic single crystal diamond detector for dosimetry in spatially fractionated synchrotron x-ray fields, Med. Phys. 43 (7) (2016) 4283–4293. doi:10.1118/1.4953833.
URL http://dx.doi.org/10.1118/1.4953833http://scitation.aip.org/content/aapm/journal/medphys/43/7/10.1118/1.4953833http://dx.doi.org/10.1118/1.4953833{%}5Cnhttp://scitation.aip.org/content/aapm/journal/medphys/43/7/10.1118/1.4953833

[11] M. Petasecca, A. Cullen, I. Fuduli, A. Espinoza, C. Porumb, C. Stanton, A. H. Aldosari, E. Bräuer-Krisch, H. Requardt, A. Bravin, V. Perevertaylo, A. B. Rosenfeld, M. L. F. Lerch, X-Tream: a novel dosimetry system for Synchrotron Microbeam Radiation Therapy, J. Instrum. 7 (07). doi:10.1088/1748-0221/7/07/P07022.
URL http://stacks.iop.org/1748-0221/7/i=07/a=P07022?key=crossref.8d1255d7745abc72cb917ba74e51af5f

[12] R. Lewis, Medical applications of synchrotron radiation in Australia, Nucl. Instruments Methods Phys. Res. Sect. A Accel. Spectrometers, Detect. Assoc. Equip. 548 (1-2) (2005) 23–29. doi:10.1016/j.nima.2005.03.061.
URL http://linkinghub.elsevier.com/retrieve/pii/S0168900205006455

[13] A. W. Stevenson, J. C. Crosbie, C. J. Hall, J. Livingstone, J. E. Lye, Quantitative characterisation of the X-ray beam at the Australian Synchrotron Imaging and Medical Beamline (IMBL)*, J. Synchrotron Radiat.

[14] J. C. Crosbie, P. A. W. Rogers, A. W. Stevenson, C. J. Hall, J. E. Lye, T. Nordström, S. M. Midgley, R. A. Lewis, C. J. Hall, T. Nordström, T. Nordstrom, S. M. Midgley, R. A. Lewis, Reference dosimetry at the Australian Synchrotron's imaging and medical beamline using free-air ionization chamber measurements and theoretical predictions of air kerma rate and half value layer, Med. Phys. 40 (6) (2013) 062103. doi:10.1118/1.4803675.
URL http://www.ncbi.nlm.nih.gov/pubmed/23718601

[15] P. Fournier, J. C. Crosbie, I. Cornelius, P. Berkvens, M. Donzelli, A. H. Clavel, A. B. Rosenfeld, M. Petasecca, M. L. F. Lerch, E. Bräuer-Krisch, Absorbed dose-to-water protocol applied to synchrotron-generated x-rays at very high dose rates, Phys. Med. Biol. 61 (14) (2016) N349–N361. doi:10.1088/0031-9155/61/14/N349.
URL http://stacks.iop.org/0031-9155/61/i=14/a=N349?key=crossref.b21be6b72c72498aeda4bb561d34fd26

[16] P. Fournier, I. Cornelius, M. Donzelli, H. Requardt, C. Nemoz, M. Petasecca, E. Bräuer-Krisch, A. Rosenfeld, M. Lerch, X-Tream quality assurance in synchrotron X-ray microbeam radiation therapy, J. Synchrotron Radiat. 23 (5) (2016) 1180–1190. doi:10.1107/S1600577516009322.
URL http://scripts.iucr.org/cgi-bin/paper?S1600577516009322